Low-Power Acoustic Trapping and Illumination Optimization of Cyanobacteria by Acoustic Layering in Photobioreactors

Bérénice Dupont[a,b], Xavier Benoit-Gonin[b], Sébastien Vincent-Bonnieu[c], Jean-Luc Aider[b*], and Maxime Ardré[a*]

[a]Laboratoire de Biophysique et Evolution (LBE), UMR8231 CNRS, ESPCI Paris - PSL, Chimie Biologie Innovation, PSL University, Paris, France

[b]Laboratoire de Physique et Mécanique des Milieux Hétérogènes (PMMH), UMR736 CNRS, ESPCI Paris - PSL, PSL University, Sorbonne University, Paris, France

[c]European Space Research and Technology Centre (ESTEC), European Space Agency (ESA), Noordwijk, The Netherlands

[*]These authors contributed equally to this work.

Abstract

Space missions necessitate sustainable life support systems capable of producing oxygen and biomass under microgravity conditions. This study examines the use of acoustic levitation to trap and manipulate the filamentous cyanobacterium *Limnospira indica* PCC 8005 during parabolic flight experiments. We demonstrate that this helicoidal microorganism can be rapidly assembled into thin layers with a standing ultrasonic wave within a millimeter-scale fluidic chamber. Our findings indicate that significantly lower acoustic power is required under microgravity (0.79 mW) compared to terrestrial conditions (1.48 mW) to achieve stable trapping, suggesting energy-efficient bioprocessing in weightless environments. Monte Carlo simulations and light attenuation modelling reveal that structuring cyanobacteria into layered formations enhances light penetration, potentially overcoming the "compensation point" limitation observed in bulk cultures. These results pave the way for advanced photobioreactors that use acoustic manipulation, which improves photosynthetic efficiency and reduces energy consumption for oxygen generation and biomass production in space.

Introduction

Space exploration and human spaceflight have been central goals for national space agencies but have risen in importance in the last decade due to the new non-governmental companies like SpaceX and Blue Origin. A key focus lies in enabling long-term space missions and establishing permanent extraterrestrial bases, first on the moon (NASA's Artemis project) and then on Mars (SpaceX), both of which rely on the development of advanced environmental control and life support systems[1]. Over the past 30 years, significant progress has been made in recycling carbon dioxide (CO_2) and water in the International Space Station (ISS)[2,3]. Beyond, the European Space Agency (ESA) initiated the MELiSSA (Micro-Ecological Life Support System Alternative) project in 1987 to design and develop a bioregenerative life support closed loop for long-duration space missions to supply food, oxygen, and water (potable and hygienic) while efficiently recycling waste[4–7].

To this goal, microalgae and cyanobacteria are considered promising candidates due to their photosynthetic capabilities[8]. Cyanobacteria are photosynthetic prokaryotes that can convert CO_2 into biomass meanwhile simultaneously releasing O_2 as a secondary product[9]. Among them, *Limnospira indica* PCC 8005 is a well-established

model organism in the MELiSSA project[10,11]. In liquid culture, this cyanobacterium forms multicellular filaments — so-called trichomes — made of cells joined end to end. Its adaptability to space conditions is well documented[12,13]. It can fulfil a dual role: first, as a biological, renewable system for O_2 production via photosynthesis and, second, as a source of edible biomass[14], contingent on sufficient light and carbon availability to sustained growth. Thus, to achieve their efficient cultivation, it is crucial to optimize the photobioreactors.

A photobioreactor is a closed system designed to cultivate light-dependent organisms under controlled environments. In this device, light absorption and scattering are key processes that influence how light propagates through the culture and reaches every microorganism. On one hand, light is absorbed by the media resulting in an exponential decrease of light as a function of the light-path in the fluid (Beer-Lambert law). On the other hand, scattering redirects light in different directions when it encounters small objects like particles or microorganisms. Several models have been developed to describe light penetration in cultures of photosynthetic microorganisms that take into account both light absorption and scattering effects[15–17]. One of the conclusions is that all of the incident light on the photobioreactor is typically extinct after the first centimeters in the culture.

The decrease in light intensity available to a cyanobacterium in a photobioreactor is quantified by the so-called *compensation point*, which is the distance from the light source where the light intensity falls below the minimum intensity needed for photosynthesis[16]. Beyond this point, the cyanobacteria no longer receive sufficient light to maintain photosynthetic activity, which slows or stops growth, thus limiting the production of biomass and the conversion of CO_2 into O_2. The position of this point in a photobioreactor depends on: the cell concentration; the photobioreactor geometry; the illumination configuration; as well as the cell absorption and scattering properties. To increase photosynthesis, one would find a solution to change the position of the compensation point by illuminating a maximum number of cells.

Acoustic levitation offers contact-free control of microscopic objects in fluids. A standing ultrasonic wave, generated by a transducer in a resonant cavity, creates an acoustic radiation force (ARF) that drives suspended particles toward the pressure nodes of the field[18,19]. Because the node pattern is fixed, the ARF localize precisely the particles along the cavity height[20–22]. Previous studies have demonstrated the ability of the ARF to trap spherical objects like particles, cells or microalgae into stable clusters[23–26]. However, its application to control the spatial distribution of living cyanobacteria for functional purposes, like light access, remains unexplored. The efficiency of the acoustic trapping depends on parameters such as the voltage and frequency applied to the ultrasonic transducer, as well as external forces (gravity, fluid acceleration). Most theoretical models describing ARF have been developed for inert, spherical[18,27–30] or elongated particles[31–35] that are small compared to the acoustic wavelength (Rayleigh hypothesis). However, *L. indica* PCC 8005 are long (about the acoustic wavelength), thin, helicoidal, soft rods that are biologically active, thereby deviating significantly from these assumptions. Although chemically fixed *L. indica* with glutaraldehyde has been levitated previously[36], considerable uncertainty remains regarding the response of *L. indica* to the ARF. Therefore, we had to show that acoustic trapping is effective for living *L. indica*— as their metabolism relentlessly shifts cytoplasmic composition and alters their mass density and compressibility. Thus, in the context of spaceborne application, two important questions need to be explored to implement this technology. First: Can ARF effectively trap living *L. indica* PCC 8005? Second: What level of electrical power is required to achieve stable acoustic trapping for different gravitational environments?

Here we demonstrate that a standing ultrasonic wave can gather *L. indica* at pressure nodes, stacking them into thin, cell-dense layers separated by clear fluid gaps. These gaps act as optical windows, allowing light to reach depths that remain dark in a fully mixed suspension. Monte-Carlo photon-transport simulations confirm

that the layered arrangement increases the fluence rate throughout the reactor, improving light availability for a larger number of cells. We then quantify trap performance in a flight-qualified millifluidic chip, measuring the drive voltage required to form and maintain the layers at 0 g during parabolic-flight as well as 1 g in the laboratory. In microgravity, the power threshold is roughly half that on Earth, showing that milliwatt-level input is sufficient for continuous operation in space. Collectively, the results identify acoustic levitation as a low-energy method for structuring cyanobacterial cultures and enhancing their utilization in future life-support systems.

Methods

Acoustic Levitation in Resonant Cavities

Acoustic waves within a resonant cavity make possible the trapping of objects in a liquid medium without any physical contact. Figure 1 illustrates the core principles of this technique. Let's consider spherical objects (particles, cells, microorganisms) initially homogeneously distributed within a fluid that fills a cavity (Fig. 1 a). If an ultrasonic transducer is located at the top of the cavity and emits an acoustic wave inside the cavity toward the lower wall of the cavity, which behaves as a rigid reflector, and if the appropriate acoustic wavelength λ_{ac} is chosen, such as $\lambda_{ac}/2$ a multiple of the cavity height h ($h = n\,\frac{\lambda_{ac}}{2}$, where $n \in \mathbb{N}^*$), then an acoustic standing wave is formed (Fig. 1 b). With this condition satisfied, one ($n = 1$) or more ($n > 1$) pressure nodes appear along the cavity's height, spaced at intervals of $\Delta z = \lambda_{ac}/2$, where z is the longitudinal direction of the wave in the same axial direction as the body of the ultrasonic transducer.

Once a standing wave is established, any object within the fluid experiences the so-called Acoustic Radiation Force (ARF). For a spherical, compressible particle much smaller than the acoustic wavelength, i.e. $d_p \ll \lambda_{ac}$, the axial component of ARF F_{rad} can be expressed as[18,27]:

$$\vec{F}_{\text{ac}} = \frac{\pi}{12}\langle E_{ac}\rangle k d_p^3 \phi \sin(2kz)\,\vec{e}_z\,, \tag{1}$$

where $\langle E_{ac}\rangle$ is the acoustic energy density, $k = 2\pi/\lambda_{ac}$ is the wavenumber, ϕ is the acoustic contrast factor, and z is the axial position of the particle.

The acoustic contrast factor ϕ characterizes the difference in mechanical properties between the particle and the surrounding fluid:

$$\phi = \frac{5\rho_p - 2\rho_f}{2\rho_p + \rho_f} - \frac{\beta_p}{\beta_f}\,, \tag{2}$$

where ρ_p and ρ_f are the densities of the particle and fluid, respectively, and β_p and β_f are their respective compressibilities. Particles with a positive acoustic contrast factor ($\phi > 0$) are driven towards the pressure nodes of the standing wave field (as indicated by the force $\vec{F}_{\text{ac}}$ in Fig. 1). Once they have reached the closest pressure node, they can be maintained in acoustic levitation as long as needed. Typical forces range from a few pN to about 0.01 pN[37]. For instance, a 10 µm diameter polystyrene bead in water (ρ_p = 1.05 g.cm^{-3}, β = 1.6 $\times$ 10^{-10} Pa^{-1}, ϕ = 0.24) subjected to an acoustic energy density of 10 J.m^{-3} experiences an ARF of about 2$\times$10^{-12} N (2 pN). This force is one order of magnitude larger than the weight of the bead. Buoyancy force is F_b = 5.13 pN and the weight is P = 5.39 pN, P-F_b = 0.79 pN.

Once the particles reach the levitation plane, they are slowly drawn toward the center of the cavity by the radial

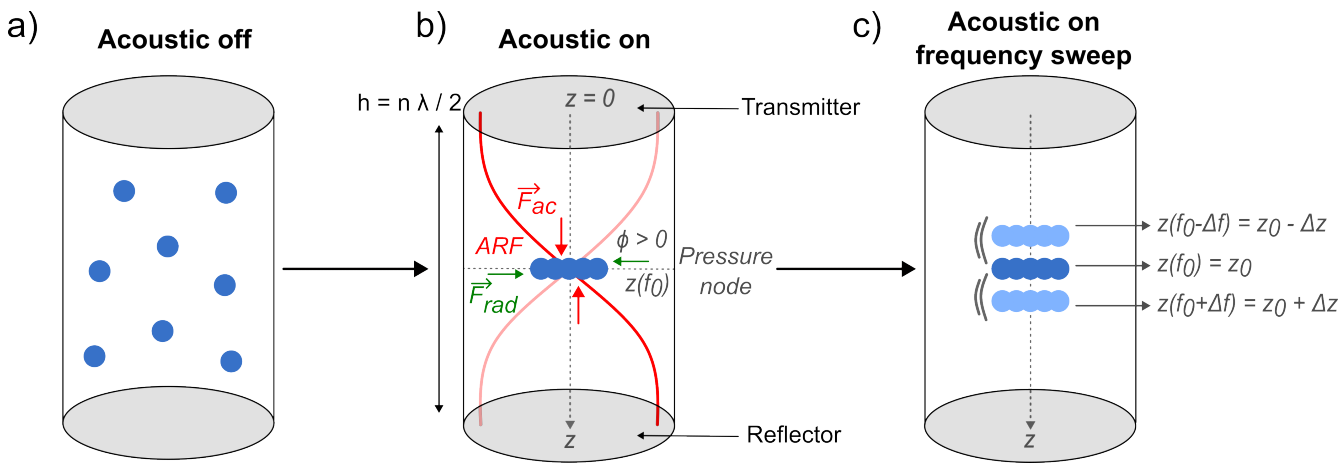

Figure 1: **Principle of Acoustic Levitation in a Resonant Cavity. a)** Particles (blue) with a positive contrast factor ($\phi > 0$) are initially uniformly distributed in the fluid-filled cavity. **b)** When the ultrasonic transducer is activated at frequency f_{ac}, the particles migrate toward the pressure node and aggregate at this stable levitation plane. In this example, $h = \lambda_{ac}/2$. **c)** Varying the acoustic frequency near resonance (f_0) leads to a displacement of the axial position of the levitation plane. A frequency change Δf_{ac} corresponds to a displacement Δz of the levitation plane, enabling precise vertical positioning of the trapped particles.

component of the ARF, $\vec{F}_{\text{rad}}$, which is much weaker (10 to 100 times weaker) than the axial component of the ARF[37] and is often neglected.

Two key acoustic parameters govern the effectiveness of acoustic levitation: first, the acoustic energy density, $\langle E_{ac} \rangle$ which depends on the square of the voltage U_{trans} applied to the transducer ($\langle E_{ac} \rangle \propto U_{trans}^2$) up to the transducer's operational limits[20,38], second, the acoustic wavelength λ_{ac} (or equivalently the acoustic frequency $f_{ac} \times \lambda_{ac} = c$, c being the celerity of sound in the fluid medium), which determines the axial position of the pressure nodes if the resonance condition is satisfied.

In a multi-nodes configuration ($n > 1$) it has been shown[21,22] that the z-position of the levitation plane can be moved along the longitudinal (z) direction by changing (slightly) the acoustic frequency. Using this property, small variations of frequency Δf_{ac} around the resonance frequency f_0 lead to small variations Δz around the node axial position at the resonance z_0, as shown in Fig. 1 c). By sweeping the frequency within a range $[f_0 - \Delta f, f_0 + \Delta f]$, one can move objects in levitation along the z-axis around the equilibrium position at the resonance ($[z_0 - \Delta z, z_0 + \Delta z]$). This oscillation of the levitation plane is possible only if the axial ARF F_{ac} is strong enough over the chosen frequency range.

Cyanobacteria typically have a positive acoustic contrast factor and should accumulate at the pressure nodes, as illustrated in Fig. 1. By adjusting both the voltage applied to the transducer while varying the acoustic frequency near f_0 it becomes possible to identify the minimum power needed to reliably trap cyanobacteria in acoustic levitation.

Millifluidic chip

The chip comprises a PDMS structure bonded to a microscope glass slide. The design of the milli-fluidic chip is shown in figure 2a. The inner dimensions of the cavity are 14 mm $\times$ 10 mm $\times$ 3 mm (length $\times$ width $\times$ height). The key feature of the chip is the height of its central cavity h_1 = 3 mm (Fig. 2 b). The total height H of the chip

corresponds to the sum of the cavity height h_1 and the height of the PDMS layer h_2 of about 0.7 mm, leading to H = 3.7 mm. The coupling between the PDMS chip and the transducer is achieved by a thin layer of oil, as illustrated in Fig. 2 b). The fabrication of the millifluidic chip begins with the preparation of a 10:1 mixture of polydimethylsiloxane (PDMS) elastomer base and curing agent (Sylgard 184). This mixture is subjected to vacuum degassing to remove any trapped air bubbles. After degassing, the mixture is carefully poured into molds and cured at 70℃ for 2 hours. Once curing is complete, the chips are gently extracted from the molds. Inlet and outlet wells are manually punched using a 2.0 mm diameter piece cutter. Both the PDMS chips and microscope glass slides are cleaned with isopropanol to ensure optimal adhesion. Finally, the PDMS pads are bonded to the glass slides via plasma treatment (20 W, 50 Hz, 8 sscm O_2).

Cyanobacteria suspended in a nutrient medium are introduced through the inlet into the central cavity of the chip using a pipette tip. The inlet and outlet are then sealed.

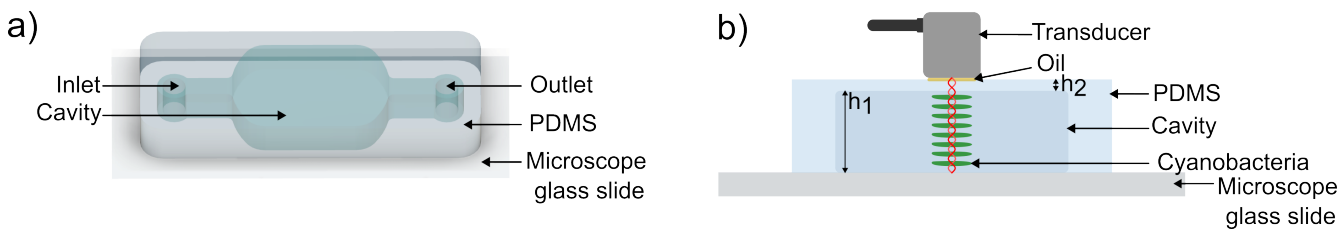

Figure 2: **Acoustofluidic chip design. a)** CAD model of the chip, showing the inlet, outlet, and central cavity. **b)** Schematic of the millifluidic chip containing a cyanobacterial culture organized in layers localized at the nodes of the resonant cavity. The transducer is mounted above the cavity. The red waving lines depict the acoustic standing waves in the cavity. The green layers illustrate the aggregation of the cyanobacteria that cluster at the nodes of the wave. A typical scale is given by h_1 which is 3 mm long.

Acousto-fluidic setup

A compact Signal Processing™(TR0205RSX) acoustic transducer, with a diameter of 5 mm and a body length of 21 mm, is placed on the top of the cavity to generate the ultrasonic wave. A thin layer of oil between the transducer and the PDMS is used to match their impedance. The transducer is powered by a Tie-Pie USB wave generator (Handyscope HS5 XM). Both the voltage and the frequency are controlled using the Tie-Pie software. To create an acoustic standing wave, we selected an operating frequency of 2.0 MHz, corresponding to an acoustic wavelength of $\lambda_{ac} \approx 740$ µm in water, which leads to the formation of 8 pressure nodes along the cavity's height (z-axis). Once the acoustic standing wave is formed, the objects in suspension migrate toward the closest pressure node, as illustrated in Fig. 2b and form layers.

To evaluate the efficiency of the acoustic trap as a function of the acoustic energy density (proportional to U_{trans}^2), a linear frequency sweep is applied from 1.8 to 2.2 MHz with a 450 ms duration cycle. The frequency sweep leads to the oscillation of the axial position of the clusters, provided that the acoustic energy density is high enough.

Experimental setup in the AirZeroG plane

Our setup, adapted from previous studies[34,39], is securely installed in a waterproof container that is firmly mounted inside the aircraft (Fig. 3a). To prevent fluid leakage, the system is kept sealed during the flights. The chip

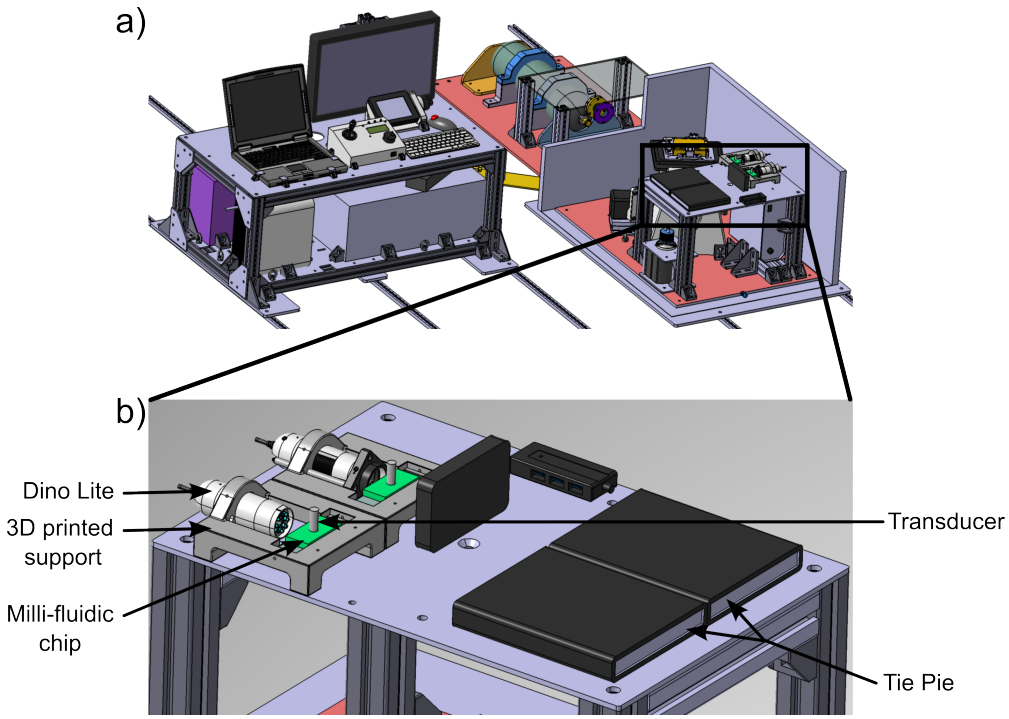

Figure 3: **3D view of the experimental setup. a)** Full view of the experimental setup, including a second rack used to control all the experimental parameters. Two experimental devices were installed. A Zeiss inverted microscope (on the left side) for cell biology experiments and milli-fluidic chips to trap cyanobacteria (on the right side). **b)** Zoom on the two PDMS chips that were used to trap the cyanobacteria. Digital microscopes (Dino Lite) were used to monitor the aggregation during the parabolas.

is housed in a 3D-printed structure designed to securely hold the transducer, the chip, and a Dino-Lite™mini-microscope (AM2111) for side observation of the chip (Fig. 3 b). The wave generator and the digital microscope are controlled by a laptop mounted on a dedicated rack (Fig. 3 a). The other elements shown in Fig. 3a are used for another unrelated experiment, which is not discussed in this article.

Each flight typically consists of six sets of five parabolas, for a total of 30 periods of microgravity of about 22 s each. Throughout the flight, the sealed box can be opened a few minutes after take-off before the first parabola for about 5 min and then six times at every break of 5 min in between the series of parabolas. This constraint prevents any modification to be applied to the device during the experiment (for example, shaking or refilling).

Limnospira indica PCC 8005

The multicellular, filamentous cyanobacteria *Limnospira indica* PCC 8005 was purchased from the Pasteur Culture Collection (PCC). The organism was cultivated in 150 ml of a nutritive Zarrouk's medium (Tab. 1) under aerobic conditions at 27℃, with an illumination intensity of 38 $\mu mol \cdot m^{-2} \cdot s^{-1}$ (equivalent to 2050 lux). Flasks were incubated in a rotary shaker set at 140 rpm. The experiments were conducted with an optical density (OD) of approximately 0.1, measured at 750 nm (optical wavelength). When needed, a sample is taken from the batch culture and injected into the chip to perform the experiments.

Measurements of the shape and size of PCC8005 in these conditions were performed for cultures of optical

Table 1: Zarrouk medium[40] composition, including trace elements.

Medium Ingredients	**Concentration ($g \cdot L^{-1}$)**
NaCl	1.0
$CaCl_2$	0.04
K_2HPO_4	0.5
$NaNO_3$	2.5
$NaHCO_3$	5.0
K_2SO_4	1.0
$MgSO_4$	0.1
$FeSO_4$	0.01
EDTA	0.08
Traces elements (A5) with Co	1 mL
Traces elements (A5) with Co	**Concentration ($g \cdot L^{-1}$)**
H_3BO_3	2.86
$MnCl_2$	1.81
$ZnSO_4$	0.222
$NaMoO_4$	0.390
$CuSO_4$	0.079
$Co(NO_3)_2$	0.049

density 0.2 (OD_{750}). Samples from batch culture were placed on a Malassez cell and imaged with a Zeiss inverted microscope at 5X in bright-field. The length and the width of every filament (or trichomes) are quantified with Fiji.

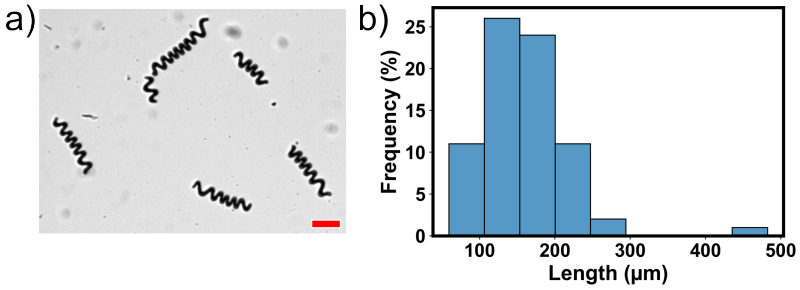

Figure 4: **Morphological characterization of *L. indica*. a)** Micrograph of *L. indica* PCC 8005 filaments. Scale bar, 50 µm. **b)** Size distribution of *Limnospira indica* PCC 8005 in liquid suspension (n = 75).

Image Analysis

Levitated-layer motion was filmed with a Dino-Lite AM2111 USB microscope (640 × 480 px, 20 fps) that was rigidly fixed to the millifluidic chip holder. AVI stacks were opened in Fiji as 8-bit gray scale and cropped to a 200-px-wide window centred on the targeted layer. A 20-px-wide vertical line region of interest was then passed through the layer's midpoints, to get the profile of intensity along the line. The z-coordinate of the uppermost dark pixel within this line -representing the highest point of the cyanobacterial layer—was measured on each frame to produce a height-versus-time trace (z(t)) in Matlab. When the acoustic radiation force is strong enough, z(t) displayed periodic oscillations. For each measurement at a given driving voltage U_{ac}, we extract the mean peak-to-peak amplitude and its standard deviation for trace lasting 11 s. A static noise of 12 µm served as the detection limit; amplitudes

below 12 µm were therefore classified as "no oscillation".

Results

Acoustic levitation of cyanobacterial trichomes

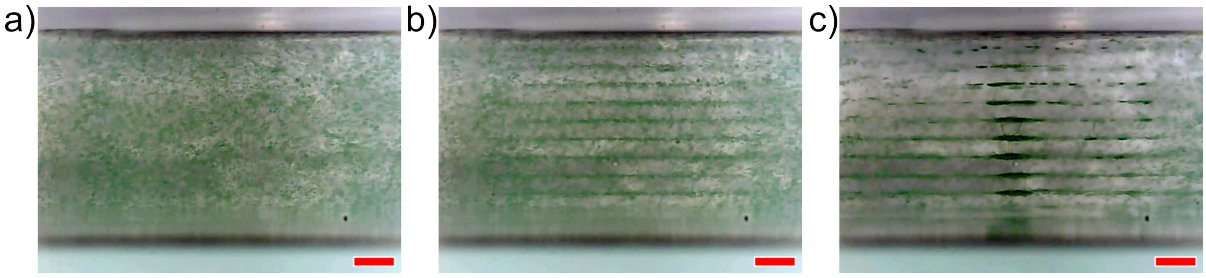

Figure 5: **Formation of layers of *Limnospira indica* PCC 8005 using acoustic levitation. a)** Initially dispersed cyanobacteria prior to acoustic field activation (green particles). **b)** Formation of layers of cyanobacteria 0,5 s after activation of the acoustic field. **c)** Formation of clusters of cyanobacteria in the central region of the cavity 15 s after activation. Scale bars, 1 mm.

The acoustic trapping of micrometric particles is well described by theory which assumes that particles are approximately spherical, and much smaller than the acoustic wavelength (750 µm in our setup)[21,23,41]. Under our experimental conditions, the cyanobacterial filaments (or trichomes) of *L. indica* PCC 8005 exhibits a spiral, rod-like morphology (Fig. 4a), with lengths ranging from 100 µm to 200 µm (length distribution in Fig. 4b) and a mean width of 25 µm.

The effective trapping of *Limnospira indica* PCC8005 by ARF is demonstrated in the Fig. 5. The cyanobacterial culture is introduced into the millifluidic chip (Fig. 2) and then the ultrasonic transducer is switch on. Fig. 5 a) - c) show that the clustering process occurs in two distinct phases. Initially, the strongest z-component of the ARF (F_{ac}) acts on the suspended cyanobacteria (Fig. 5b), rapidly forming (within 0.5 s) multiple layers at the pressure nodes of the multinode resonant cavity (Fig. 5c). Subsequently, after approximately 15 s (Fig. 5d), aggregates begin to form at the center of each layer, driven by the weaker radial component of the ARF (F_{rad}). It results in compact, layer-like clusters with a thickness along the z-axis of about 100 µm and a lateral width of approximately 1 mm. These observations demonstrate that live, helicoidal cyanobacteria—despite their complex geometry and time-varying material properties—can be stably trapped, layered, and repositioned with acoustic forces.

Furthermore, Fig. S1 in the supplementary shows that acoustic levitation does not affect cellular viability. A culture subjected to levitation for 6 hours demonstrate growth comparable to a culture that had not undergone levitation.

Therefore, the spontaneous formation of alternating layers of biomass and transparent medium offers an appealing design for light management in photobioreactors.

Acoustic layering enhances light distribution in cyanobacterial photobioreactors

While conventional photobioreactors rely on suspended cultures regularly agitated to provide light to every the cell, we propose to take advantage of the ARF for spatially organizing the cyanobacterial culture into layers, thereby

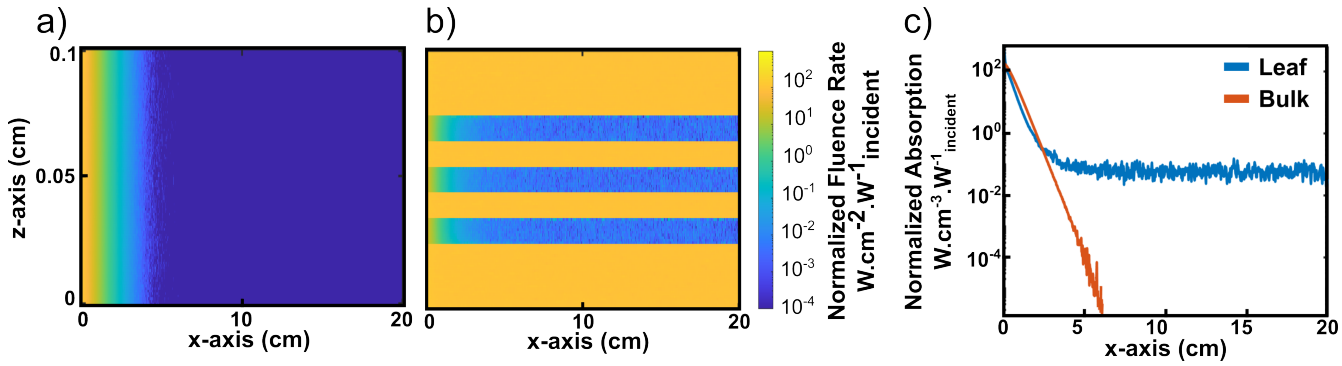

Figure 6: **Monte Carlo simulations of light distribution in a photo-bioreactor with and without layering of cyanobacterial culture. a)** Fluence rate of light in a vertical slice of a bulk culture where cyanobacteria are suspended. The light source is located at x = 0. **b)** Fluence rate of light in a vertical slice when cyanobacteria are trapped at the acoustic nodes, forming three distinct layers of cyanobacteria interspaced by layers of transparent fluid. Note that the scales of the z-axis and x-axis are not the same for readability. a) and b) share the same z-axis. **c)** Mean normalized absorption profiles along the x-axis when the cyanobacteria are distributed homogenously (bulk) or organized in horizontal layers (leaf).

opening optical "windows" through the reactor.

To test whether acoustically induced layering alleviates the limitation of the *compensation point*[16], we ran photon-transport simulations with *MCmatlab*[42]. Two geometries were compared: Bulk - cells are uniformly distributed at C_x = 1 kg·m^{-3}; Leaf - cells are organized in three layers of 100 µm thickness (cell density 3.33 kg·mm^{-3} to conserve biomass) separated by transparent fluid (Fig.,6b) that mimics experiment Fig. 5. Both simulations use the same absorption coefficients (E_a) scattering coefficients (E_s), and g coefficient as the Cornet model[43]. A top-hat beam entered at $x = 0$ with a slight angle ($\arctan(L_z/L_x)$) and crossed the domain (L_z = L_y = 0.1 cm and L_x = 20 cm). Light exiting through the opposite side at $x = Lx$ is considered lost. Cyclic boundary conditions are applied on the sides (plane at z = 0 z = L_z, y = 0, y = L_y), meaning that a photon exiting through one boundary re-enters through the opposite boundary. Figures 6a–b map the resulting fluence-rate fields. Fig.6c plots the mean absorbed power density versus light path. The absorption is averaged on the full height of the cavity L_z for the "bulk" culture and averaged only on the pixels within the layers for the "leaf" culture.

In the bulk case the flux collapses to zero within 6 cm, confirming the classical *compensation point* bottleneck. In the layered architecture the flux decays but stabilise at a finite value beyond 4 cm because photons that traverse through clear gaps are still available to excite the layers. In other words, layering redistributes light more uniformly through the photobioreactor potentially keeping every cyanobacteria above the threshold required for photosynthesis. Having established how acoustic layering improves light delivery, we next quantify the electrical cost of maintaining those layers under 0 g and 1 g.

Performance of the acoustic trap under 0 g and 1 g

To determine the minimum electrical power required for stable trapping in microgravity, we boarded a flight-qualified millifluidic chip into the Novespace Air Zero-G aircraft. Each parabola provides 22 s of 0 g micro-g phase, bracketed by 1.8 g pull-up/pull-out of hyper-g phases. Before take-off the chip is loaded with a *L. indica* suspension, and the transducer is driven at 2 MHz, 10 V to hold the cells during the hyper-g phase. Once 0 g phase is reached, the

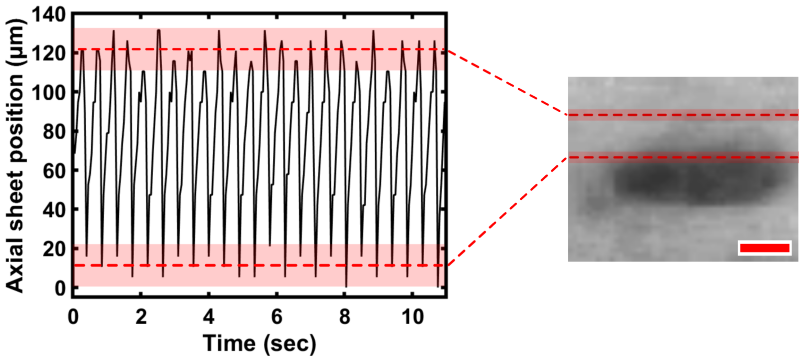

Figure 7: **Axial oscillations of acoustically levitated *L. indica* PCC 8005 layers.** Right: Cropped video frame captured during a 0 g parabola, showing a cyanobacterial layer held at a pressure node. The red dashed lines show the extremal positions of the uppermost pixel of that layer during its up and down displacement. Left: Time trace of the z-position of the uppermost pixel of that layer, recorded at a voltage U_{ac} = 5 V. The black curve gives the instantaneous position; red dashed lines mark the mean of the maxima and minima; the red shaded bands denote plus or minus s.d. around those means. Scale bar, 100 µm.

driving voltage (U_{ac}) is stepped to the tested value, as the voltage is directly linked to the strength of the ARF (see Eq. 1). Then the frequency is swept from 1.8 to 2.2 MHz (450 ms cycle). This sweep shifts the pressure nodes; if the acoustic radiation force (ARF) is strong enough, the cyanobacterial layers follows the node and oscillates along the z-axis (see Fig. 1). The layer's z-position is extracted from video (ImageJ) and converted to oscillation amplitude in MATLAB. Figure 7 illustrates a typical 0-g run: the right panel shows the levitated layer, and the left panel plots its z-position over time. Oscillation amplitude was defined as the mean peak-to-peak displacement; values below the 12-µm noise like in the supplementary Fig. S4 were scored as zero in the following analysis. Eleven-second traces were collected for U_{ac} between 0.3 and 10 V in micro-g. We also performed the same experiment in the laboratory at 1 g but this time the voltage spanned in the range of 1 V to 10 V.

Figure 8 shows how oscillation amplitude varies with voltage (the supplementary Fig. S2 shows the same plot with power as x-axis). In micro-g the first detectable oscillations appear at 0.8 V, grow quasi-linearly to 4 V, and then plateau at 100 µm. Under 1 g the threshold shifts rightward to 1.8 V; above that point, the curve follows a similar slope but saturates at roughly half the micro-g amplitude. Below 1.8 V gravity overwhelms the acoustic radiation force (ARF) and the layers sediments. The voltage–power calibration (Supplementary Fig. S3) translates the 0 g threshold into 0.79 mW and the 1 g threshold into 1.48 mW—modest in both cases, but twice as high on Earth. Microgravity therefore halves the power requirement while doubling the controllable stroke, enabling large-amplitude positioning.

Taken together, the data demonstrate that low-power acoustic tweezers can stably trap, translate, and concentrate filamentous cyanobacteria under space-relevant conditions. This capability paves the way for creating photobioreactors that operate without the need for stirrers and pumps while providing controlled light distribution and on-demand biomass harvesting. This makes them an appealing option for high-reliability, energy-efficient life-support systems beyond low-Earth orbit.

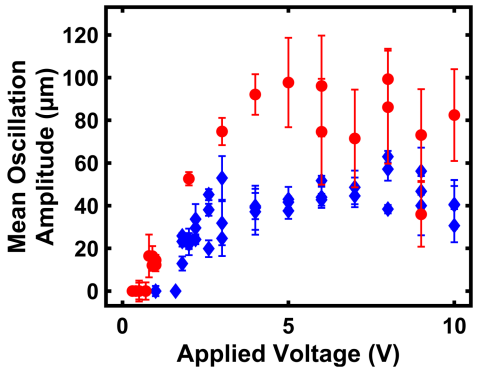

Figure 8: **Mean oscillation amplitude of a *Limnospira indica* PCC 8005 sheet as a function of transducer voltage.** Blue diamonds represent the 1 g condition, while red circles correspond to 0 g conditions. The points are the mean amplitude oscillation, while the error bars are the standard deviation around the mean.

Discussion

In this study we show that acoustic levitation allows to reposition living, spiral *L. indica* filaments in both 1 g and 0 g environments. The ARF stacks the cells into stable layers, creating clear gaps that let light reach deep into the culture.

Layering overcomes the classic *compensation point* bottleneck: each layer are illuminated over their entire surface, ensuring every cell sees light. In contrast, conventional photobioreactors rely on continuous agitation to keep cells suspended and sweep them through the illuminated zone, yet vigorous mixing still leaves inner regions starved of photons[43]. Crucially, the power drawn for acoustic trapping falls from 1.48 mW at 1 g to just 0.79 mW in microgravity, since no force has to balance the weight. A small piezoelectric transducer can thus run uninterrupted aboard a spacecraft without straining the station's power. Meanwhile, a typical 12 V motor at 15 rpm consumes about 300 mW to stir a liter of culture. Although our chip volume is far below a litre, layered assemblies of microbes have already been demonstrated over 8 cm paths, indicating that decimetres-deep reactors are attainable with the same kind of small transducer [26]. Moreover, the passive stability of our layers, which persists long after the field is switched off in microgravity (no sedimentation), further reduces energy demand.

The lighting configuration of the photobioreactor is a critical parameter. The simulations indicate that, in the layered configuration, approximately 67% of the incident light exits the photobioreactor through the $x = 0$ or $x = L_x$ boundaries, while only 33% is absorbed by the cyanobacterial layers. In contrast, bulk cultures absorb 100% of the light within the first few centimeters. To optimize light illumination, implementing reflective walls within the device could reduce light loss. Additionally, the type of illumination significantly affects light distribution. Beam illumination is more effective than isotropic illumination in minimizing shadow effects and ensuring that the light reaches the entire layer. Adjusting the angle between the light beam and the layers axis is also crucial to minimize shading effects. These parameters still need optimization and experimental validation to effectively maximize light utilization in layered photobioreactors.

Trapping the filaments in stationary layers has potentially an additional benefit: it permits gentle, low-shear perfusion that removes dissolved O_2 before it accumulates to growth-inhibiting levels. In simulated-microgravity experiments with *L. indica*, Ellena et al.[44] observed that the absence of convection produces a thick, stagnant boundary layer around the cells; oxygen released during photosynthesis then builds up locally and slows growth.

Because our acoustic trap keeps each layer fixed in space, a weak, steady medium flux can be directed across the layers without breaking them apart, continuously flushing excess O_2 while still operating at milliwatt power. In this way acoustic layering potentially mitigates one of the main physiological constraints reported for cyanobacterial cultures in microgravity[44,45].

Further understanding of the ARF applied to cyanobacteria requires more refined models. Previous theoretical approaches, such as those by Marston et al.[32], Mitri et al.[33], Silva & Drinkwater[46], and Leao et al.[35], have primarily focused on spherical or simple-shaped elongated particles. Complex behaviors observed with metallic nanorods, such as self-acoustophoresis (autonomous propulsion of the nanorods) in the acoustic levitation plane due to interactions between the acoustic wave and the rods, have been reported[34,47]. However, such motions have not been observed with cyanobacteria, likely due to their much lower density compared to metallic particles.

Harvesting cyanobacteria cultivated in photobioreactors is critical to be able to use them. Acoustic levitation can also accelerate the process by enhancing the sedimentation[26]. Other methods propose to rely on ARF to separate biomaterials under terrestrial gravity and microgravity conditions using an h-shaped ultrasonic resonator[36]. In this study, we demonstrate an additional phenomenon: the ARF's ability to relocate cyanobacterial clusters to different sites within the medium. This feature can be leveraged to optimize the harvesting, especially in environments where there is no sedimentation.

Finally, scaling up acoustic levitation for larger photobioreactors, such as a 50 cm deep reactor, necessitate to assess the required power. The energy demand scales with the volume and acoustic field strength. Therefore careful consideration is needed to balance trapping efficiency with power consumption. Future work will explore scaling up the photobioreactor and measuring changes in oxygen production under acoustic levitation. Besides, understanding how the dimensions of the reactor influence the photosynthetic efficiency will be key to design scalable systems.

At last, layered culture in photobioreactors reduces operational complexity and energy consumption while also mitigating mechanical wear and contamination hazards associated with moving parts. As a result, it is a prospective technique for considerably increasing the feasibility of bioprocessing in space, enabling longer-duration missions with more sustainable biomass production and CO_2 recycling.

Code and data availability

All relevant data and codes are available upon demand.

Aknowledgement

The authors wish to thank ESA and the Carnot IPGG for funding the PhD thesis of B. Dupont. The participation in the parabolic flights campaign was financially supported by the CNES (French Aerospace Agency). The authors thank G. Gauquelin-Koch (in charge of the Life Science topic at the CNES) and T. Brett-Dibat (in charge of the Matter Science topic at the CNES).

Author contribution

B.D., X.B-G., J-L.A. and M. A.: conception and fabrication of the setup. B.D., J-L.A. and M.A.: conceptualization and methodology. B.D., J.-L.A. and M.A.: samples preparation, data acquisition, analysis and simulations. B.D.,

S.B-V., J.-L.A. and M.A.:writing original draft, review and editing. S.B-V., J.L.A. and M.A.: supervised the project. All authors contributed to the article and approved the submitted version.

Competing interest

The author declare no competing interest.

Additional information

Correspondence and requests should be addressed to jean-luc.aider@espci.psl.eu and maxime.ardre@espci.psl.eu.

References

1. Gentry, G. J. & Cover, J. *International Space Station (ISS) Environmental Control and Life Support (ECLS) System Overview of Events: 2010–2014* in *45th International Conference on Environmental Systems* (Bellevue, Washington, 2015).

2. Witt, J., Hovland, S. & Bockstahler, K. *ACLS - Europe's Closed Loop Air Revitalisation System* in *40th International Conference on Environmental Systems* (2010). doi:10.2514/6.2010-6232.

3. Bockstahler, K., Lucas, J. & Witt, J. *Design Status of the Advanced Closed Loop System ACLS for Accommodation on the ISS* in *43rd International Conference on Environmental Systems* (Vail, Colorado, 2013). doi:10.2514/6.2013-3450.

4. Hendrickx, L., De Wever, H., Hermans, V., Mastroleo, F., Morin, N., *et al.* Microbial ecology of the closed artificial ecosystem MELiSSA (Micro-Ecological Life Support System Alternative): reinventing and compartmentalizing the Earth's food and oxygen regeneration system for long-haul space exploration missions. *Res. Microbiol.* **157,** 77–86. doi:10.1016/j.resmic.2005.06.014 (2006).

5. Farges, B., Poughon, L., Creuly, C., Cornet, J.-F. & Lasseur, C. Dynamic Aspects and Controllability of the MELiSSA Project: A Bioregenerative System to Provide Life Support in Space. *Appl. Biochem. Biotechnol.* **151,** 686–699. doi:10.1007/s12010-008-8292-2 (2008).

6. Lasseur, C. *MELiSSA: The European project of a closed life support system* in *Gravitational and Space Biology* (2008).

7. Walker, J. & Granjou, C. MELiSSA the minimal biosphere: Human life, waste and refuge in deep space. *Futures* **92,** 59–69. doi:10.1016/j.futures.2016.12.001 (2017).

8. Poughon, L., Laroche, C., Creuly, C., Dussap, C.-G., Paille, C., *et al.* Limnospira indica PCC8005 growth in photobioreactor: model and simulation of the ISS and ground experiments. *Life Sci. Space Res.* **25,** 53–65. doi:10.1016/j.lssr.2020.03.002 (2020).

9. Ciferri, O. Spirulina, the Edible Microorganism. *Microbiol. Rev.* **47,** 551–578. doi:10.1128/mr.47.4.551-578.1983 (1983).

10. Soreanu, G., Cretescu, I., Diaconu, M., Cojocaru, C., Ignat, M., *et al.* Investigation of a biosystem based on Arthrospira platensis for air revitalisation in spacecrafts: Performance evaluation through response surface methodology. *Chemosphere* **264,** 128465. doi:10.1016/j.chemosphere.2020.128465 (2021).

11. Garcia-Gragera, D., Peiro, E., Arnau, C., Cornet, J.-F., Dussap, C.-G., *et al.* Dynamics of long-term continuous culture of Limnospira indica in an air-lift photobioreactor. *Microb. Biotechnol.* **15,** 931–948. doi:10.1111/1751-7915.13882 (2022).

12. Cogne, G., Cornet, J.-F. & Gros, J.-B. Design, Operation, and Modeling of a Membrane Photobioreactor to Study the Growth of the Cyanobacterium Arthrospira platensis in Space Conditions. *Biotechnol. Prog.* **21,** 741–750. doi:https://doi.org/10.1021/bp0495926 (2005).

13. Badri, H., Monsieurs, P., Coninx, I., Nauts, R., Wattiez, R., *et al.* Temporal Gene Expression of the Cyanobacterium Arthrospira in Response to Gamma Rays. *PLoS One* **10,** 1–29. doi:10.1371/journal.pone.0135565 (2015).

14. Habib, M., Parvin, M., Huntington, T. & Hasan, M. *A review on culture, production, and use of Spirulina as food for humans and feeds for domestic animals and fish* FAO Fisheries and Aquaculture Circular No. 1034 (FAO, Rome, Italy, 2008).

15. Cornet, J. F., Dussap, C. G. & Dubertret, G. A structured model for simulation of cultures of the cyanobacterium Spirulina platensis in photobioreactors: I. Coupling between light transfer and growth kinetics. *Biotechnol. Bioeng.* **40,** 817–825. doi:10.1002/bit.260400709 (1992).

16. Cornet, J.-F., Dussap, C. G. & Gros, J.-B. in *Bioprocess and Algae Reactor Technology, Apoptosis* 153–224 (Springer Berlin Heidelberg, Berlin, Heidelberg, 1998). doi:10.1007/BFb0102299.

17. Ma, S., Huang, Y., Zhang, B., Zhu, X., Xia, A., *et al.* Comprehensive modeling and predicting light transmission in microalgal biofilm. *J. Environ. Manage.* **326,** 116757. doi:10.1016/j.jenvman.2022.116757 (2023).

18. Bruus, H. Acoustofluidics 7: The acoustic radiation force on small particles. *Lab Chip* **12,** 1014–1021. doi:10.1039/C2LC21068A (2012).

19. Lenshof, A., Evander, M., Laurell, T. & Nilsson, J. Acoustofluidics 5: Building microfluidic acoustic resonators. *Lab Chip* **12,** 684–695. doi:10.1039/C1LC20996E (2012).

20. Dron, O. & Aider, J.-L. Acoustic energy measurement for a standing acoustic wave in a micro-channel. *Europhys. Lett.* **97,** 44011. doi:10.1209/0295-5075/97/44011 (2012).

21. Dron, O. & Aider, J.-L. Varying the agglomeration position of particles in a micro-channel using Acoustic Radiation Force beyond the resonance condition. *Ultrasonics* **53,** 1280–1287. doi:10.1016/j.ultras.2013.03.012 (2013).

22. Jeger-Madiot, N., Mousset, X., Dupuis, C., Rabiet, L., Hoyos, M., *et al.* Controlling the force and the position of acoustic traps with a tunable acoustofluidic chip: Application to spheroid manipulations. *J. Acoust. Soc. Am.* **151,** 4165–4179. doi:10.1121/10.0011464 (2022).

23. Evander, M. & Nilsson, J. Acoustofluidics 20: Applications in acoustic trapping. *Lab Chip* **12,** 4667–4676. doi:10.1039/C2LC40999B (2012).

24. Jeger-Madiot, N., Arakelian, L., Setterblad, N., Bruneval, P., Hoyos, M., *et al.* Self-organization and culture of mesenchymal stem cell spheroids in acoustic levitation. *Sci. Rep.* **11,** 8355. doi:10.1038/s41598-021-87459-6 (2021).

25. Rabiet, L., Arakelian, L., Jeger-Madiot, N., García, D. R., Larghero, J., *et al.* Acoustic levitation as a tool for cell-driven self-organization of human cell spheroids during long-term 3D culture. *Biotechnol. Bioeng.* **121,** 1421–1433. doi:10.1002/bit.28651 (2024).

26. Bellebon, L., Levant, M., Hoyos, M. & Aider, J.-L. Accelerating particle aggregation in acoustic levitation by collective effects: Application to cost-effective ultrasonic harvesting of microalgae. *Phys. Rev. Appl.* **23,** 014006. doi:10.1103/PhysRevApplied.23.014006 (2025).

27. Yosioka, K. & Kawasima, Y. Acoustic Radiation Pressure on a Compressible Sphere. *Acustica* **5,** 167–173 (1955).

28. Doinikov, A. A. Acoustic radiation pressure on a rigid sphere in a viscous fluid. *Proc. R. Soc. Lond. A* **447,** 447–466. doi:10.1098/rspa.1994.0150 (1994).

29. Baresch, D., Thomas, J.-L. & Marchiano, R. Three-dimensional acoustic radiation force on an arbitrarily located elastic sphere. *J. Acoust. Soc. Am.* **133,** 25–36. doi:10.1121/1.4770256 (2013).

30. Silva, G. T. Acoustic radiation force and torque on an absorbing compressible particle in an inviscid fluid. *J. Acoust. Soc. Am.* **136,** 2405–2413. doi:10.1121/1.4895691 (2014).

31. Wei, W., Thiessen, D. B. & Marston, P. L. Acoustic radiation force on a compressible cylinder in a standing wave. *J. Acoust. Soc. Am.* **116,** 201–208. doi:10.1121/1.1753291 (2004).

32. Marston, P. L., Wei, W. & Thiessen, D. B. *Acoustic radiation force on elliptical cylinders and spheroidal objects in low frequency standing waves* in *AIP Conference Proceedings* **838** (2006), 495–499. doi:10.1063/1.2210403.

33. Mitri, F. Acoustic radiation force on a rigid elliptical cylinder in plane (quasi) standing waves. *J. Appl. Phys.* **118,** 214903. doi:10.1063/1.4936617 (2015).

34. Dumy, G., Jeger-Madiot, N., Benoit-Gonin, X., Mallouk, T. E., Hoyos, M., *et al.* Acoustic manipulation of dense nanorods in microgravity. *Microgravity Sci. Technol.* **32,** 1159–1174. doi:10.1007/s12217-020-09835-7 (2020).

35. Leao-Neto, J. P., Hoyos, M., Aider, J.-L. & Silva, G. T. Acoustic radiation force and torque on spheroidal particles in an ideal cylindrical chamber. *J. Acoust. Soc. Am.* **149,** 285–295. doi:10.1121/10.0003046 (2021).

36. Böhm, C., Jenke, D. & Gerlach, J. Quantification of a novel H-shaped ultrasonic resonator for separation of biomaterials under terrestrial gravity and microgravity conditions. *Biotechnol. Bioeng.* **82,** 74–85. doi:10.1002/bit.10546 (2003).

37. Dumy, G., Hoyos, M. & Aider, J.-L. Observation of selective optical manipulation of particles in acoustic levitation. *J. Acoust. Soc. Am.* **146,** 4557–4568. doi:10.1121/1.5139640 (2019).

38. Barnkob, R., Augustsson, P., Laurell, T. & Bruus, H. Measuring the local pressure amplitude in microchannel acoustophoresis. *Lab Chip* **10,** 563–570. doi:10.1039/B920376A (2010).

39. Lecoq, P.-E., Dupuis, C., Mousset, X., Benoit-Gonnin, X., Peyrin, J.-M., *et al.* Influence of microgravity on spontaneous calcium activity of primary hippocampal neurons grown in microfluidic chips. *npj Microgravity* **10,** 15. doi:10.1038/s41526-024-00355-x (2024).

40. Zarrouk, C. *Contribution à l'étude d'une cyanophycée: Influence de divers facteurs physiques et chimiques sur la croissance et la photosynthèse de Spirulina maxima* PhD thesis (University of Paris, 1966).

41. Laurell, T. & Lenshof, A. *Microscale Acoustofluidics* doi:10.1039/9781849737067 (Royal Society of Chemistry, 2014).

42. Marti, D., Aasbjerg, R. N., Andersen, P. E. & Hansen, A. K. MCmatlab: an open-source, user-friendly, MATLAB-integrated three-dimensional Monte Carlo light transport solver with heat diffusion and tissue damage. *J. Biomed. Opt.* **23,** 121622. doi:10.1117/1.JBO.23.12.121622 (2018).

43. Cornet, J.-F. *Procédés Limités par le Transfert de Rayonnement en Milieu Hétérogène* Habilitation à Diriger des Recherches. 2007.

44. Ellena, G., Fahrion, J., Gupta, S., Dussap, C. G., Mazzoli, A., *et al.* Development and implementation of a simulated microgravity setup for edible cyanobacteria. *npj Microgravity* **10.** doi:10.1038/s41526-024-00436-x (2024).

45. Fahrion, J., Renaud, C., Coninx, I., Heylen, W., Mastroleo, F., *et al.* ARTHROSPIRA-C space flight experiment: Validation of biomass and oxygen production bioprocesses in a space bioreactor prior to upload to space. *Acta Astronaut.* **229,** 374–390. doi:10.1016/j.actaastro.2024.11.010 (2025).

46. Silva, G. T. & Drinkwater, B. W. Acoustic radiation force exerted on a small spheroidal rigid particle by a beam of arbitrary wavefront: Examples of traveling and standing plane waves. *J. Acoust. Soc. Am.* **144,** EL453–EL459. doi:10.1121/1.5080529 (2018).

47. Wang, W., Castro, L. A., Hoyos, M. & Mallouk, T. E. Autonomous motion of metallic microrods propelled by ultrasound. *ACS nano* **6,** 6122–6132. doi:10.1021/nn301312z (2012).

Supplementary data

Cell after levitation acoustic exposure

To ensure that acoustic levitation do not kills the cells, we measure the growth of *L. indica* PCC 8005 prior and following exposure to acoustic levitation. We used an alternative setup, a custom-designed stainless steel resonant cavity with dimensions of 55 mm in height, length, and width. The cavity featured watertight lateral poly(methyl methacrylate) (PMMA) windows and a threaded ring for mounting of the ultrasonic transducer (Olympus™, model A395S).

Cell growth was monitored by optical dentisy (OD_{750}) prior to the exposure, after 6 hours of exposure to acoustic levitation, and subsequently at 48 and 168 hours post-incubation in standard culture condition, described in the main text of the article. No impact on growth is evident after acoustic exposure.

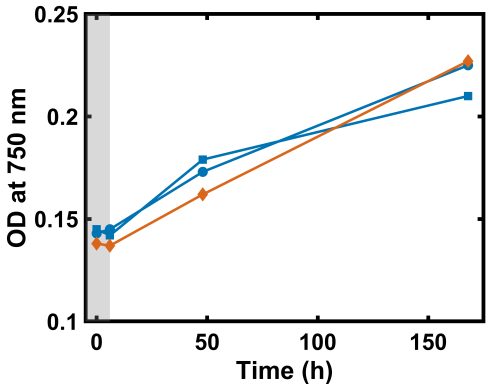

Figure S1: **Monitoring the growth of *Limnospira indica* PCC 8005 before and after exposure to acoustic levitation.** The blue curves represent levitated cells, with circles and squares indicating two distinct replicates, whereas the orange curve indicates control cells that were not subjected to sonic levitation. Cells were subjected to acoustic levitation between 0 and 6 hours, as indicated by the shaded area. Then, cell growth was subsequently monitored under standard conditions from 6 to 168 hours.

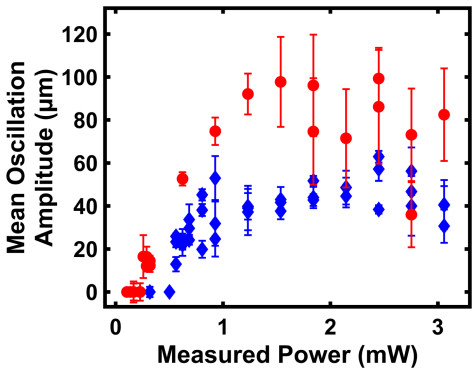

Figure S2: **Mean fluctuations of *Limnospira indica* PCC 8005 sheet under acoustic levitation as a function of the power delivered to the transducer.** The blue diamonds represent the mean oscillations of the sheet under 1 g conditions, whereas the red circles indicate the mean oscillations of the sheet under 0 g conditions.

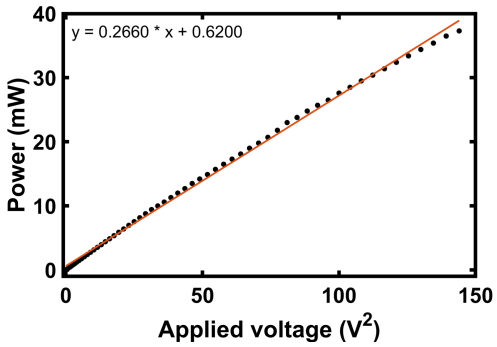

Figure S3: **Correlation between applied voltage (V^2) and electric power emitted by the Tie-Pie™ device.** The black circles represent the measured data, while the orange line indicates the linear fit, described by the equation $y = 0.2260 \cdot x + 0.6200$.

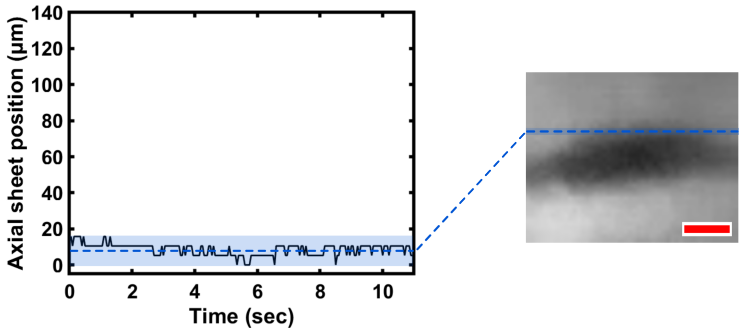

Figure S4: **Example of a non-oscillating aggregate at 0.3 V under microgravity.** The black curve shows the evolution of the vertical position of the aggregate at 5 V under microgravity over time. Blue dotted lines indicate the average value of the detected peaks of the respective maximum and minimum displacement amplitudes. The blue shaded region represents the standard deviation of the aggregate's oscillations around the averaged values. Scale bar, 100 µm.